Nanocrystallized layer formed by sliding wear under high stress for pure Cu

Hisashi Sato*, Ryo Tsuzuki, Yuya Kaneko, and Yoshimi Watanabe

Department of Engineering Physics, Electronics and Mechanics, Graduate School of Engineering, Nagoya Institute of Technology, Nagoya 466-8555, Japan

E-mail: sato.hisashi@nitech.ac.jp

When metallic materials become worn, a nanocrystallized layer is often observed under the worn surface. This layer is called the wear-induced layer (WIL). In this study, the mechanism behind the formation of the WIL by sliding wear under high stress for pure Cu is investigated. The microstructure around the worn surface changes discontinuously between the WIL and the plastically deformed region (PDR). The grain size in the WIL is much smaller than that in the PDR, whereas grains in the PDR underneath the WIL are refined by huge strain due to wear. From the results of crystallographic texture analysis, the WIL has recrystallization texture, whereas deformation texture with a <110> fiber is observed in the PDR. Hence, in the WIL, frictional heat causes recrystallization, which induces further grain refinement. It is concluded that the WIL is formed by both severe plastic deformation (SPD) due to wear and the recrystallization due to frictional heat.

1. Introduction

When metallic materials become worn, large shear deformation occurs on the worn surface [1-9]. As a result, a subsurface layer is formed under the worn surface [2-16]. This subsurface layer is known as the wear-induced layer (WIL). The WIL consists of nano-grains and has very high hardness. Since the WIL has a much different microstructure from the plastic deformed region (PDR), the boundary is clearly observed between the WIL and the PDR. Although the WIL is also called the white etching layer and tribolayer [1-4, 6-16], the microstructures of these layers are essentially the same.

Formation mechanisms of such WILs have been reported in previous studies [3-13, 15]. Newcomb and Stobbs investigated the microstructure of the WIL formed in a rail track surface (Fe-1 mass% Mn-0.6 mass% C-0.1 mass% Si-0.06 mass% S-0.06 mass% P alloy) by using transmission electron microscopy (TEM) [11]. According to their study [11], the WIL in the rail track surface has an apparently fully martensitic structure and is formed by the decomposition of cementite without austenitization owing to high-frequency pulse shear fatigue. On the other hand, microstructural analyses of the WIL in a rail track surface (pearlitic steel rail) by atom probe tomography and TEM have been carried out by Takahashi *et al*.[7]. In their study [7], they found that martensitic transformation after rapid austenization is the origin of the WIL. In addition to steel, the formation behavior of the WIL in Al and Cu alloys has also been reported [5, 6, 8, 9, 12, 16]. Watanabe *et al.* reported that sliding wear for Al-Al_3Ti functionally graded materials (FGMs) forms the supersaturated solid-solution layer, in which Ti is supersaturately dissolved in the Al matrix, below the worn surface [12]. In addition, Sato *et al.* mentioned that the WIL in the worn Al-Al_3Ti FGMs is generated at a nominal shear strain of more than 90 [5], and that the origin of the WIL is huge shear strain due to sliding wear. As can be seen from those previous studies, phase transformation [7, 11, 13] and large shear strain [2-5, 8, 9, 12] have been proposed as the primary formation mechanism of the WIL. Although large shear strain has recently become more popular as the primary formation mechanism, the formation mechanism of the WIL still remains unclear. As already mentioned above, the WIL has a discontinuous microstructure with PDR. However, those formation mechanisms in the previous studies [3-13] cannot explain the formation of the boundary between the WIL and the PDR. The influence of frictional heat is expected to be one of the reasons for the formation of this boundary. This means that marked grain refinement would occur locally around the worn surface by discontinuous dynamic recrystallization due to frictional heat.

To clarify the influence of the frictional heat, the investigation of the distribution

of crystallographic texture would be effective. This is because the recrystallization texture induced by heating is different from the deformation texture. In previous studies [2, 6, 14, 17, 18], crystallographic textures formed by sliding wear were examined. Wheeler and Buckley studied the textures around a surface worn by sliding wear for Cu, Ni, Fe, and Co using X-ray diffraction (XRD) [17]. According to that study, for Cu and Ni with the fcc crystal structure, the deformation texture with a <111> fiber, in which the (111) plane is parallel to the worn plane, is developed by sliding wear. On the other hand, sliding wear for Fe and Co with the bcc crystal structure forms the deformation texture with a <110> fiber. Subsequently, Krause and Demirci reported that the textures on worn surfaces of Cu and Ni specimens change markedly with increasing distance from the worn surface [2]. However, the texture analysis in those studies was carried out without classifying the WIL or PDR because of the low resolution of XRD. Therefore, the difference in texture between the WIL and the PDR is not well understood.

Recently, electron backscatter diffraction (EBSD) has often been used for the measurement of local crystallographic texture [6, 14, 19]. Although crystallographic textures around the worn surface of the Cu alloy or Ni were investigated using EBSD by Cai *et al.* [6] and Prasad *et al.*[14], they focused on the crystallographic texture formed only by wear under low stress (less than 0.1 MPa). Hence, the crystallographic texture in the WIL induced by wear under high stress, which forms a clear boundary between the WIL and the PDR, has not been studied. Sliding wear applies both shear and compressive stresses on the worn surface. The wear under high stress would be affected by compressive stress, while the influence of compressive stress under the wear with low stress would be small. According to previous studies [20-22], uniaxial compression for fcc metals such as Al and Cu generates the <110> fiber texture with the <110> axis parallel to the compression axis. Because of this, the texture formed by wear under high stress is expected to be different from that formed by wear under low stress.

In this study, the local distribution of crystallographic textures induced by sliding wear under high stress (1 MPa) for pure Cu is investigated using field emission scanning electron microscopy (FE-SEM) with EBSD. In particular, we focus on the difference in crystallographic texture between the WIL and the PDR. Referring to the obtained results, we discuss the formation mechanism of the WIL during sliding wear under high stress.

2. Experimental methods

Cold-rolled pure Cu (99.96 %) was used. Bar-shaped specimens with a 3 mm^2 wear plane

and a 15 mm height were cut from the cold-rolled pure Cu. These specimens were annealed at 600 ºC for 2 h and then mechanically polished.

Wear tests for the polished specimens were performed at room temperature using a block-on-disc wear machine. Figure 1 is a schematic illustration of the block-on-disc wear test together with specimen coordinates for microstructural observation. In the specimen coordination, SD, LD, and TD correspond to the sliding, loading, and transverse directions, respectively. This wear test is performed by putting the specimen on a rotating counter disc. The counter disc of the wear tests was made of S45C (Fe-0.45 mass% C alloy) with a Vickers hardness of HV=190. The initial stress and sliding speed were 1.0 MPa and 1.0 m/s, respectively. Moreover, sliding distances for the wear tests were 500 and 1500 m.

Cross sections of worn specimens were mechanically and chemically polished to observe the cross-sectional microstructure around the worn surface. The final chemical polishing was carried out using colloidal silica (OP-S). Microstructural observations around the worn surface were performed using optical microscopy (OM) and FE-SEM. In addition, crystal orientation analysis was carried out using EBSD. For the EBSD measurement, the acceleration voltage was 15 kV and the step size was 0.3, 0.07, or 0.05 μm. Measurement points with a confidence index (CI)>0.01 are used for analysis.

3. Results and discussion

3.1 Initial microstructure

Figures 2(a) and 2(b) are an OM photograph and a set of pole figures of the specimen before the wear test, respectively. The initial microstructure of the specimen consists of equiaxial grains. The average grain size of the specimen, which is calculated from the area, is 95 μm. From (111), (001), and (110) pole figures, the crystal orientation of the specimen before the wear test is found to be slightly rotated around the <111> or <001> axis. This means that this specimen has weak <111> and <001> fiber textures. When a Cu-based wire with deformation textures is recrystallized by annealing, <111> and <001> fiber textures are formed by high- and low- temperature annealing processes, respectively [22]. Therefore, it is seen that the specimen before the wear test has a recrystallization texture.

3.2 Microstructural change induced by sliding wear

OM photographs of the cross-sectional microstructure around the worn surface are shown in Fig. 3. White broken lines in these photos are the boundary between the WIL and the PDR. For both specimens wear-tested at sliding distances of 500 and 1500 m, the WIL is

clearly observed. The WIL is heterogeneously distributed around the worn surface. Furthermore, grains underneath the WIL are severely shear deformed.

Figure 4 is a set of SEM images showing microstructures around the worn surface in the worn specimens. In Figs. 4(a) and 4(b), left- and right-side photos are low- and high-magnification photos, respectively. These photos are electron-backscatter compositional images and show electron-channeling contrast due to the strain and crystal orientation. Moreover, coordination for microstructural observation is shown schematically beside these figures. The SEM images show the WIL as clear as the OM photographs. It is seen from these high-magnification photographs that the microstructure around the worn surface is discontinuous between the WIL and the PDR, and that a boundary is formed between these layers. As will be shown later, grain size changes discontinuously at this boundary. Moreover, since contrast changes inside a grain in the PDR, it is clear that severe shear deformation occurred in this region.

To investigate the difference in grain size between the WIL and the PDR, inverse pole figure (IPF) maps of the specimens are depicted in Fig. 5. Right and left IPF maps for each figure are low- and high-magnification maps, respectively. As shown in high-magnification IPF maps, equiaxial grains are elongated in the sliding direction, and these grains are refined at the PDR underneath the WIL. When severe plastic deformation (SPD) is induced in metallic materials, grain refinement is caused by continuous dynamic recrystallization following the grain subdivision process [5, 8, 9, 23-28]. In the case of sliding wear, large shear strain is induced around the worn surface [1-9]. Accordingly, grain refinement in the PDR just below the WIL is induced by SPD due to sliding wear.

From high-magnification IPF maps, it is seen that grain sizes for both specimens change discontinuously at the boundary between the WIL and the PDR. Average grain sizes of the WIL and PDR shown in the high-magnification maps are presented in Table I. The average grain size of the WIL is much smaller than that of the PDR. Furthermore, the grain sizes of the WIL and PDR decrease with increasing sliding distance. Therefore, it is found that further grain refinement occurred in the WIL, and that the grain refinement process in the WIL is different from that in the PDR.

3.3 Crystallographic textures in the WIL and PDR

Figures 6(a) and 6(b) are pole figures of the WIL and PDR in the worn specimen tested at a sliding distance of 500 m, respectively. In these figures, (111), (001), and (110) pole figures for each region are presented. An IPF map showing the microstructure at the

boundary between the WIL and the PDR is given in Fig. 6(c) for reference. Furthermore, inverse pole figures in the WIL and PDR analyzed from the normal direction of the boundary between these regions are shown in Figs. 7(a) and 7(b), respectively.

The crystal orientation in the PDR is slightly rotated around the <110> axis, as shown in Fig. 6(b). This means that the <110> fiber texture is formed in the PDR. From the inverse pole figure shown in Fig. 7(b), the <110> axis of this fiber texture is parallel to the normal direction of the boundary. As already mentioned in Sect. 1, the <110> fiber texture with the <110> axis parallel to the compression axis is formed as a deformation texture by uniaxial compression in fcc metals [20-22]. It is, therefore, found that the PDR has a deformation texture induced by compression along the normal direction of the boundary. On the other hand, from the pole figure and the inverse pole figure shown in Figs. 6(a) and 7(a), respectively, the <110> fiber texture remains in the WIL and the shapes of some orientation poles in the WIL become sharper than that in the PDR. This means that crystal rotation due to deformation is small in the WIL. In a previous study [21], it was revealed that the fiber texture formed by uniaxial deformation remains after primary recrystallization when a drawn Cu wire is annealed. In contrast, the texture of the <111> component becomes stronger after secondary recrystallization after annealing at high temperatures for the Cu wire [21]. Formation behaviors of these recrystallization textures are similar to the results of texture analysis for the WIL in the present study. When metallic materials are worn, high frictional heat is locally generated around the worn surface. Such frictional heat would exceed the recrystallization temperature and induce recrystallization around the worn surface. Consequently, it can be concluded that the WIL and PDR have the deformation and recrystallization textures, respectively.

Results of crystallographic texture analysis for the worn specimen at a sliding distance of 1500 m are shown in Figs. 8 and 9. These figures are the same as those in Figs. 6 and 7. The PDR has the deformation texture with the <110> fiber. Like the specimen tested at a sliding distance of 500 m, the <110> axis of this fiber texture is parallel to the normal direction of the boundary between the WIL and the PDR. Furthermore, compared with the orientation poles in the PDR, the intensities of orientation poles in the WIL are higher and the shapes of the poles become sharp. Hence, the worn specimen at a sliding distance of 1500 m has the recrystallization texture in the WIL and the deformation texture in the PDR, similarly to the specimen tested at a sliding distance of 500 m.

Between the two specimens, the specimen at the sliding distance of 1500 m has stronger textures in both the WIL and the PDR. This is because the compressive strain at

the PDR and the temperature on the worn surface increase with increasing sliding distance of the specimen. Thus, sliding wear with longer sliding distance results in the formation of stronger textures in the WIL and PDR of the worn specimen.

Wheeler and Buckley studied crystallographic textures around worn surfaces of fcc metals including pure Cu [17]. In their study, wear tests were performed under relatively low initial stress, such as 0.07 MPa, and crystallographic textures around the worn surface are evaluated by XDR. On the basis of the results of XRD analysis, they concluded that the {111} plane became parallel to the sliding plane in the wear test and a (111) texture developed. In addition to that previous study, the formation of the (111) texture in the wear test under reciprocal movement reported for pure Cu was reported by Krause and Demirci [2]. Although the results reported in those previous studies present that the textures of the PDR and WIL are overlapped owing to the low spatial resolution of XRD, these previous results are completely different from that in the present study. In particular, the PDR in our present worn specimen has the <110> fiber texture, which is often observed in a uniaxially compressed metallic sample. This is because the initial stress of wear tests in the present study is higher than those in the previous studies. If the wear test is performed under low stress, the component of compression strain induced by wear can be ignored. However, in the case of the wear test under high stress, compression strain would be too large to be ignored. This compression strain may be large in the PDR with refined grains under the WIL because the WIL has high hardness owing to its very fine structure. As a result, the <110> fiber texture is formed in this very fine-grained PDR.

3.4 Formation mechanism of the WIL

Let us here consider the formation mechanism of the WIL in pure Cu. When pure Cu is worn by the sliding wear test, shear deformation in the sliding direction occurs on the worn surface [1]. As the wear test proceeds, equiaxial grains are elongated in the sliding direction, and subsequently, grain refinement is caused by the grain subdivision process.

Onaka suggested that Hencky strain is useful in evaluating the shear strain induced by SPD [29, 30]. Hencky strain is a logarithmic strain with tensor presentation [29-32]. Using this equivalent Hencky strain, Sato *et al.* proposed a method for evaluating the shear strain induced by sliding wear using a micrograph [8]. When an equiaxial grain with a size of d is deformed into an ellipsoidal grain with the thickness t by simple shear deformation, as shown in Fig. 10, the equivalent Hencky strain $\bar{\delta}_{\mathrm{Hencky}}$ can be obtained as

$$\bar{\delta}_{\mathrm{Hencky}} \approx \frac{2\ln\left(\frac{d}{t}\right)}{\sqrt{3}} \quad (d >> t)\,. \tag{1}$$

In the case of the wear test in the present study, compressive deformation occurs in the PDR with refined grains. However, in the PDR with coarse grains, which is relatively far from the WIL, the effects of compression would be small. Assuming that the influence of compression during the wear test is small at the PDR with coarse grains, $\bar{\delta}_{\mathrm{Hencky}}$ required for grain refinement in the PDR can be calculated using Eq. (1) for the specimen tested at a sliding distance of 1500 m. As already mentioned in Sect. 3.1, the diameter of the initial equiaxial grain is d=95 μm. Moreover, the thickness of a shear-deformed grain before the grain refinement is t=1.94 μm, as shown in the right micrograph of Fig. 10. Inserting d and t into Eq. (1), $\bar{\delta}_{\mathrm{Hencky}}$ required for grain refinement in the PDR is 4.5. This means that grain refinement induced by sliding wear occurs at $\bar{\delta}_{\mathrm{Hencky}} \approx 4.5$. As one of the SPD processes, accumulative roll bonding (ARB) has often been adopted [23-28]. Onaka further derived $\bar{\delta}_{\mathrm{Hencky}}$ induced by ARB with N_{ARB} cycles [29].

$$\bar{\delta}_{\mathrm{Hencky}} = 0.8N_{\mathrm{ARB}} \tag{2}$$

From Eq. (2), the equivalent Hencky strain of 4.5 corresponds to N_{ARB}=5.6. Kamikawa *et al.* investigated the grain refinement behavior of ultra low-carbon IF steel subjected to ARB under room temperature [25]. According to that study, grains are refined by increasing the number of ARB cycles, and then, uniform ultrafine-grained structures are produced with the repetition of ARB above 5 cycles. This number is close to N_{ARB}=5.6. Hence, grain refinement in the PDR is caused by SPD due to wear.

After grain refinement in the PDR, refined grains are compressed by loading in the wear test and the <110> fiber texture is formed as the deformation texture. As the wear test further proceeds, frictional heat induces recrystallization around the worn surface. Consequently, further grain refinement occurs around the worn surface and recrystallization textures are formed. Moreover, as the sliding distance increases, grain size in the WIL decreases because the recrystallization in the WIL becomes more active owing to the larger strain in the PDR and the higher frictional heat on the worn surface. Therefore, the microstructure around the worn surface is discontinuous between the PDR and the WIL.

4. Conclusions

The mechanism of the nanocrystallized layer formation by sliding wear under high stress for pure Cu was investigated. The nanocrystallized layer was called the wear-induced layer (WIL). In this study, the formation mechanism of the WIL was discussed in terms of crystallographic textures. The main results are as follows.

(1) The grain size in the plastically deformed region (PDR) below the WIL is much smaller than the initial grain size. This grain refinement occurred with severe plastic deformation (SPD) due to wear.

(2) The PDR with refined grains has a <110> fiber texture with the <110> axis parallel to the normal direction of the boundary between the WIL and the PDR. Hence, the PDR has a deformation texture.

(3) The WIL has a recrystallization texture. This recrystallization texture is formed by frictional heat during wear. Moreover, further grain refinement is caused by the recrystallization due to frictional heat. As a result, the grain size in the WIL is much smaller than that in the PDR with refined grains, and the microstructure around the worn surface is discontinuous between the WIL and the PDR.

(4) The WIL with nanocrystallized grains is formed by SPD due to wear and recrystallization due to frictional heat.

Acknowledgments

This work is supported by “Grant-in-Aid for Scientific Research C (25420753)” from the Ministry of Education, Culture, Sports, Science and Technology of Japan, and The AMADA Foundation. These financial supports are gratefully acknowledged.

References

1) J. H. Dautzenberg and J. H. Zatt, Wear **23**, 9 (1975).
2) H. Krause and A. H. Demirci, Wear **61**, 325 (1980).
3) P. Heilmann, H. A. T. Clark, and D. A. Rigney, Acta Metall. **31**, 1293 (1983).
4) G. Baumann, H. J. Fecht, and S. Liebelt, Wear **191**, 133 (1996).
5) H. Sato, T. Murase, T. Fujii, S. Onaka, Y. Watanabe, and M. Kato, Acta Mater. **56**, 4549 (2008).
6) W. Cai, J. Mabon, and P. Bellon, Wear **267**, 485 (2009).
7) J. Takahashi, K. Kawakami, and M. Ueda, Acta Mater. **58**, 3602 (2010).
8) H. Sato, E. Miura-Fujiwara, and Y. Watanabe, Materia Japan. **50**, 331 (2011) [in Japanese].
9) H. Sato, E. Miura-Fujiwara, and Y. Watanabe, Jpn. J. Appl. Phys. **51**, 01AK01 (2012).
10) T. S. Eyre and A. Baxter, Tribology **6**, 256 (1972).
11) S. B. Newcomb and W. M. Stobbs, Mater. Sci. Eng. **66**, 195 (1984).
12) Y. Watanabe, N. Yamanaka, and Y. Fukui, Metall. Mater. Trans. **30A**, 3253 (1999).
13) W. Österle, H. Rooch, A. Pyzalla, and L. Wang, Mater. Sci. Eng. A **303**, 150 (2001).
14) S. V. Prasad, J. R. Michael, and T. R. Christenson, Scr. Mater. **48**, 255 (2003).
15) H. W. Zhang, S. Ohsaki, S. Mitao, M. Ohnuma, and K. Hono, Mater. Sci. Eng. A **421**, 191 (2006).
16) A. Emge, S. Karthikeyan, and D. A. Rigney, Wear **267**, 562 (2009).
17) D. R. Wheeler and D. H. Buckley, Wear **33**, 65 (1975).
18) Z. N. Farhat, Wear **250**, 401 (2001).
19) A. J. Schwarz, M. Kumar, B. L. Adams, and D. P. Field, *Electron Backscatter Diffraction in Materials Science* (Springer, New York, 2009) 2nd ed., p. 7.
20) C. S. Barrett, *Structure of Metals* (McGraw-Hill, New York, 1952) 2nd ed., p. 446.
21) S. Nagashima, *Texture* (Maruzen, Tokyo, 1984) p. 118 [in Japanese].
22) F. J. Humphreys and M. Hatherly, *Recrystallization and Related Annealing Phenomena* (Pergamon, Oxford, U.K., 1995) pp. 53 and 335.
23) Y. Saito, N. Tsuji, H. Utsunomiya, T. Sakai, and R. G. Hong, Scr. Mater. **39**, 1221 (1998).
24) N. Hansen, Metall. Mater. Trans. A **32A**, 2917 (2001).
25) N. Kamikawa, T. Sakai, and N. Tsuji, Acta Mater. **55**, 5873 (2007).
26) N. Tsuji, Tetsu-to-Hagane **94**, 582 (2008) [in Japanese].
27) N. Tsuji and T. Maki, Scr. Mater. **60**, 1044 (2009).
28) K. Tirsatine, H. Azzeddine, T. Baudin, A.-L. Helbert, F. Brisset, B. Alili, and D. Bradai, J.

Alloys Compd. **610**, 352 (2014).

29) S. Onaka, Nihon Kinzoku Gakkaishi **74**, 165 (2010) [in Japanese].

30) S. Onaka, Philos. Mag. Lett. **90**, 633 (2010).

31) H. Hencky, Z. Tech. Phys. **9**, 215 (1928) [in German].

32) A. D. Freed, J. Eng. Mater. Technol. **117**, 379 (1995).

Figure Captions

Fig. 1. (Color online) Schematic illustration of block-on-disc wear test together with specimen coordination for microstructural observation.

Fig. 2. (Color online) (a) OM photograph and (b) (111), (001), and (110) pole figures of specimen before wear test.

Fig. 3. OM photographs showing cross-sectional microstructure around worn surface of specimens wear-tested at sliding distances of (a) 500 and (b) 1500 m. The white broken line presents the boundary between the WIL and the PDR.

Fig. 4. SEM photographs showing microstructures around worn surface of specimens wear-tested at sliding distances of (a) 500 and (b) 1500 m. These photos are backscatter electron compositional images. Left- and right-side photos in each figure are low- and high-magnification photos, respectively. Coordination for microstructural observation is shown schematically beside the SEM photographs.

Fig. 5. (Color) IPF maps showing crystal orientation distribution around worn surface of specimens wear-tested at sliding distances of (a) 500 and (b) 1500 m. Left- and right-side IPF maps in each figure are low- and high-magnification IPF maps, respectively.

Fig. 6. (Color online) (111), (001), and (110) pole figures of the (a) WIL and (b) PDR in worn specimen tested at sliding distance of 500 m. (c) IPF map showing microstructure around boundary between the WIL and the PDR in this specimen.

Fig. 7. (Color online) Inverse pole figures in the (a) WIL and (b) PDR analyzed from normal direction of the boundary between these regions for the worn specimen at sliding distance of 500 m.

Fig. 8. (Color online) (111), (001), and (110) pole figures of the (a) WIL and (b) PDR in worn specimen tested at sliding distance of 1500 m. (c) IPF map showing microstructure around boundary between the WIL and the PDR in this specimen.

Fig. 9. (Color online) Inverse pole figures in the (a) WIL and (b) PDR analyzed from normal direction of the boundary between these regions for the worn specimen at sliding distance of 1500 m.

Fig. 10. (Color online) Schematic illustration showing simple shear deformation

of an equiaxial grain together with micrograph of PDR of worn specimen with sliding distance of 1500 m.

Table I. Average grain sizes in the WIL and PDR in worn specimens.

Sliding distance of wear tests (m)	Position	Average grain size (μm)
500	WIL	0.47
	PDR	1.06
1500	WIL	0.23
	PDR	0.72

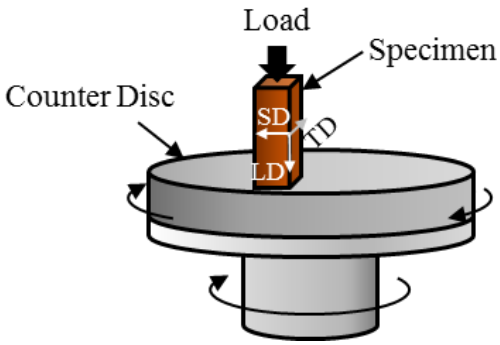

Fig. 1. (Color online) Schematic illustration of block-on-disc wear test together with specimen coordination for microstructural observation.

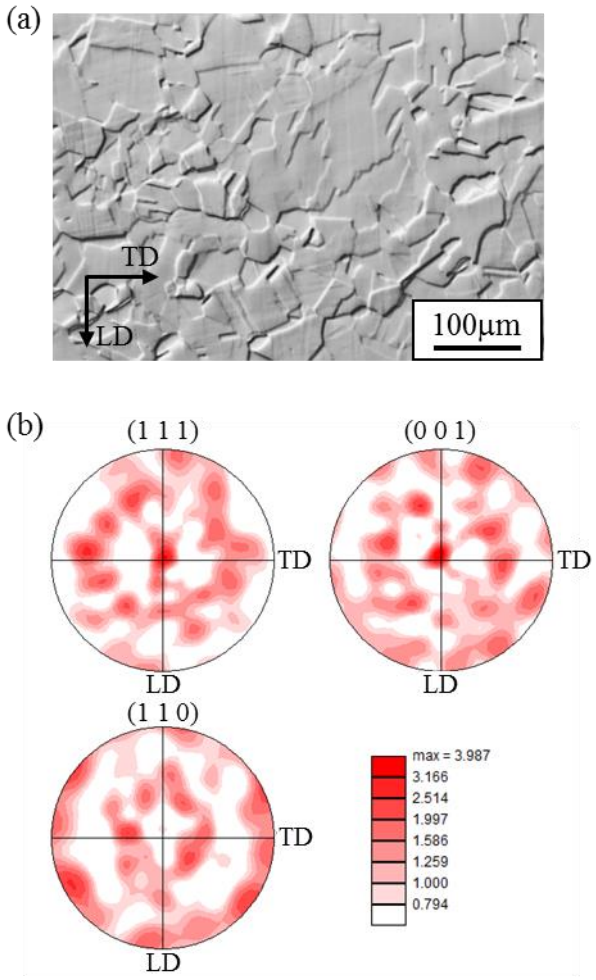

Fig. 2. (Color online) (a) OM photograph and (b) (111), (001), and (110) pole figures of specimen before wear test.

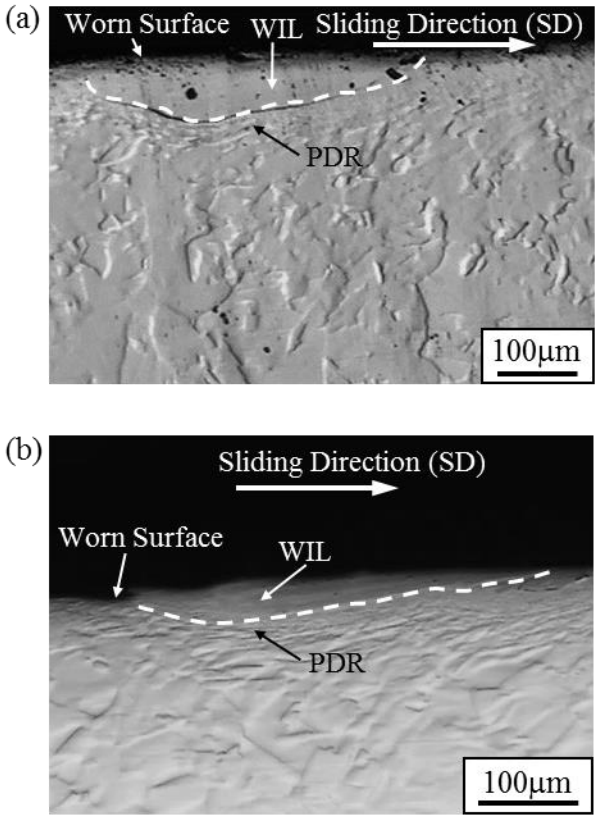

Fig. 3. OM photographs showing cross-sectional microstructure around worn surface of specimens wear-tested at sliding distances of (a) 500 and (b) 1500 m. The white broken line presents the boundary between the WIL and the PDR.

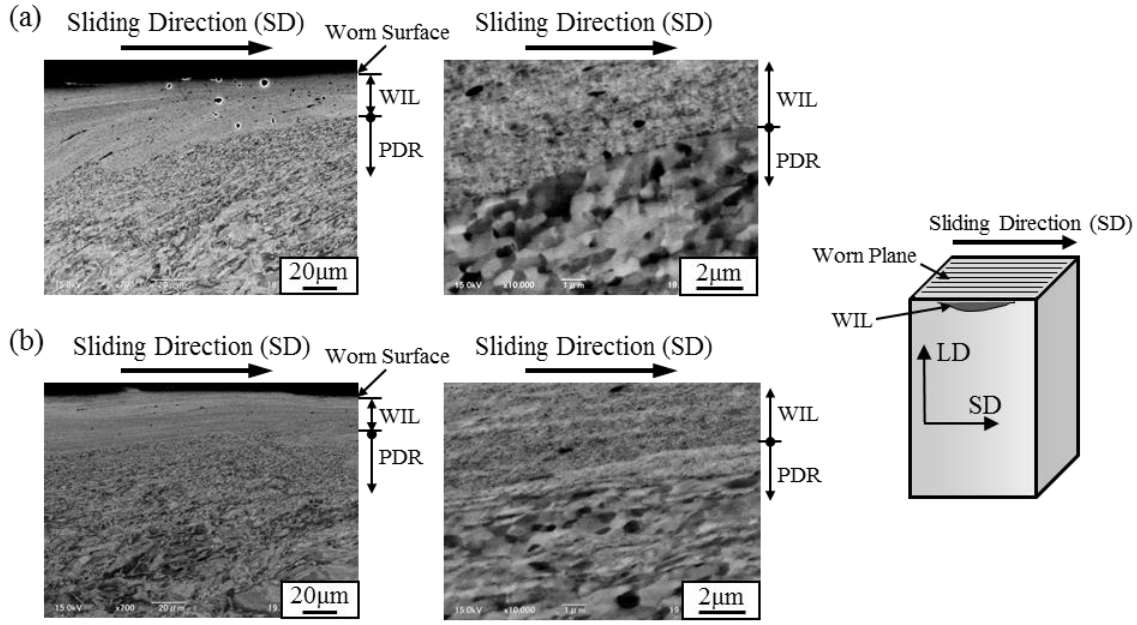

Fig. 4. SEM photographs showing microstructures around worn surface of specimens wear-tested at sliding distances of (a) 500 and (b) 1500 m. These photos are backscatter electron compositional images. Left- and right-side photos in each figure are low- and high-magnification photos, respectively. Coordination for microstructural observation is shown schematically beside the SEM photographs.

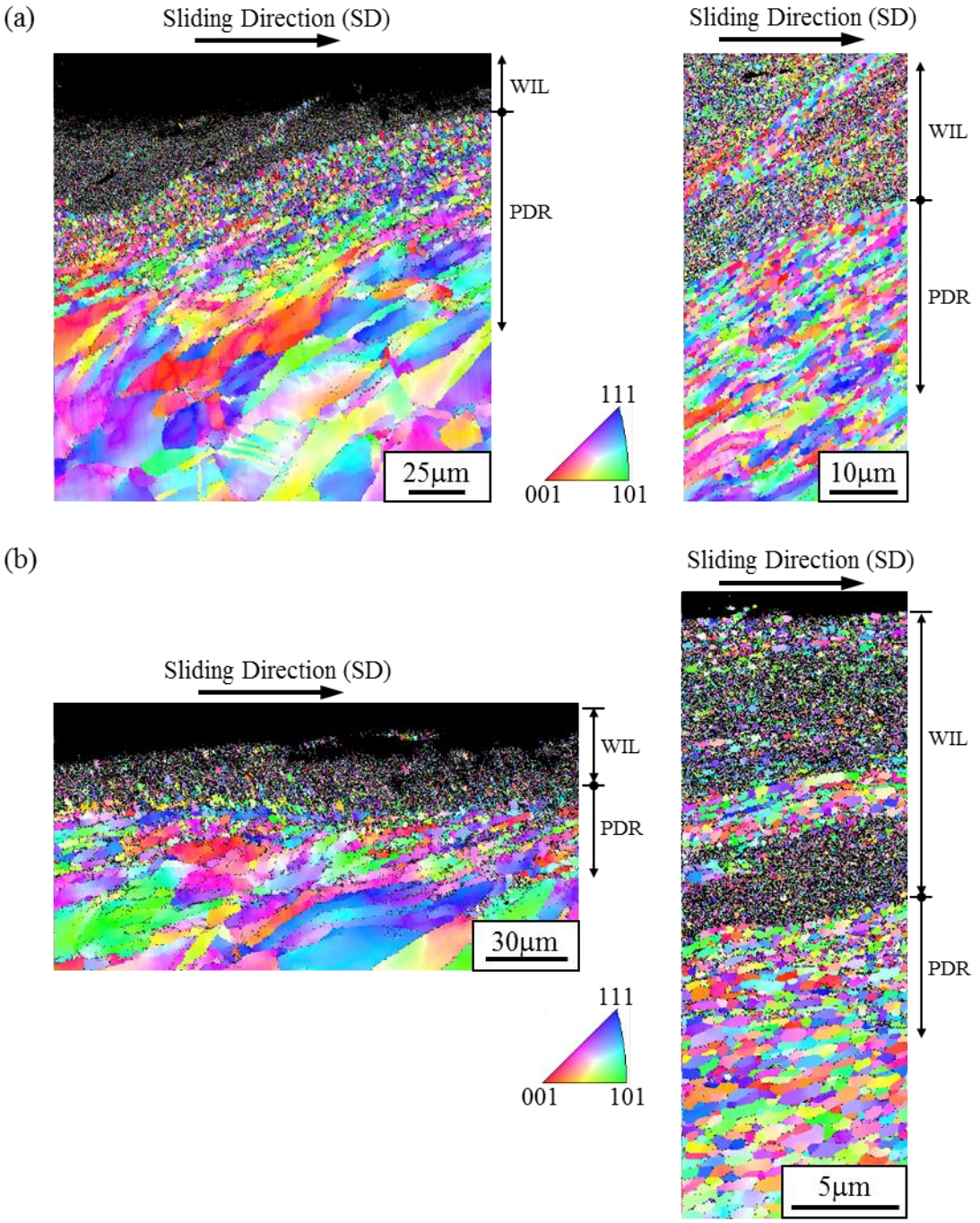

Fig. 5. (Color) IPF maps showing crystal orientation distribution around worn surface of specimens wear-tested at sliding distances of (a) 500 and (b) 1500 m. Left- and right-side IPF maps in each figure are low- and high-magnification IPF maps, respectively.

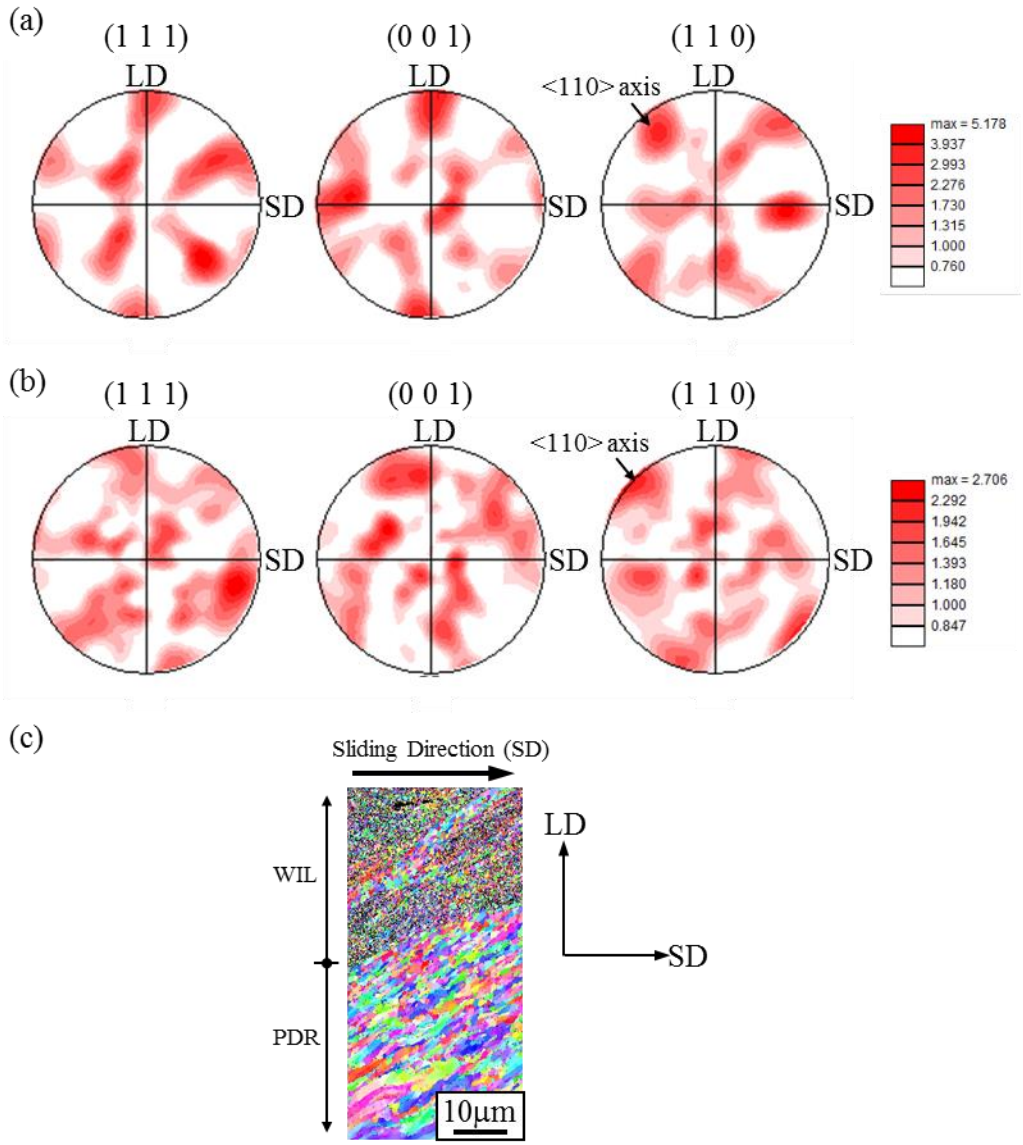

Fig. 6. (Color online) (111), (001), and (110) pole figures of the (a) WIL and (b) PDR in worn specimen tested at sliding distance of 500 m. (c) IPF map showing microstructure around boundary between the WIL and the PDR in this specimen.

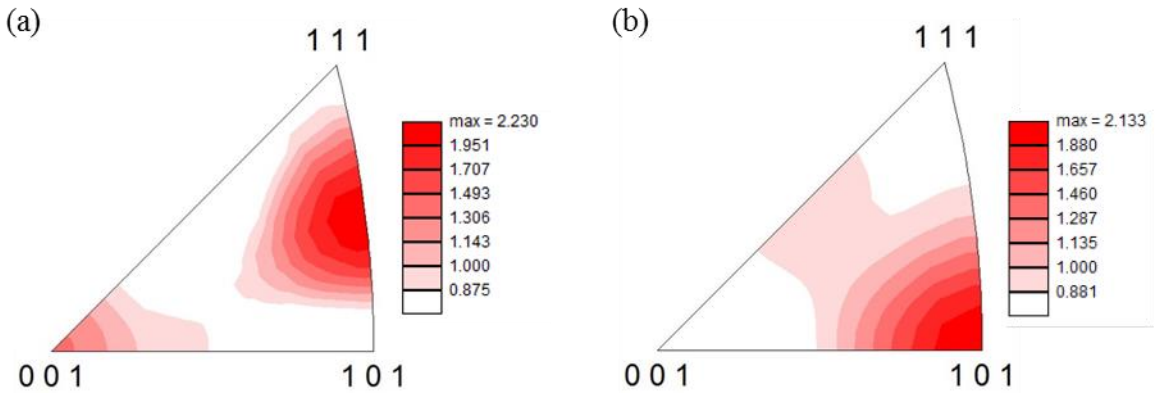

Fig. 7. (Color online) Inverse pole figures in the (a) WIL and (b) PDR analyzed from normal direction of the boundary between these regions for the worn specimen at sliding distance of 500 m.

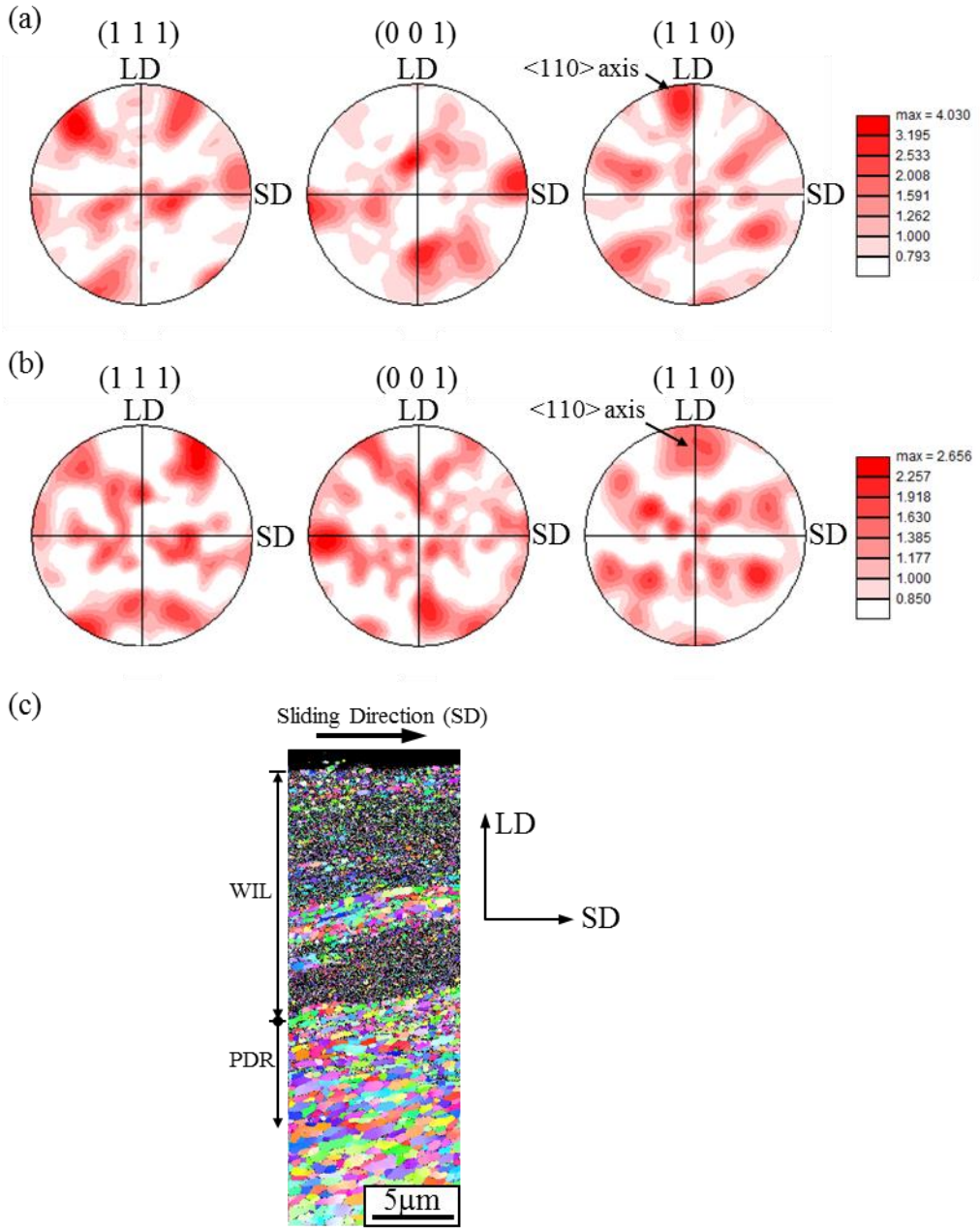

Fig. 8. (Color online) (111), (001), and (110) pole figures of the (a) WIL and (b) PDR in worn specimen tested at sliding distance of 1500 m. (c) IPF map showing microstructure around boundary between the WIL and the PDR in this specimen.

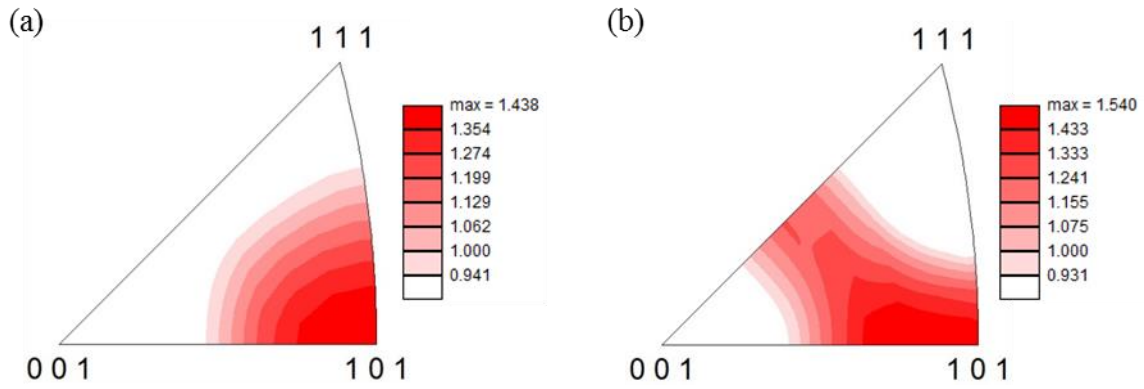

Fig. 9. (Color online) Inverse pole figures in the (a) WIL and (b) PDR analyzed from normal direction of the boundary between these regions for the worn specimen at sliding distance of 1500 m.

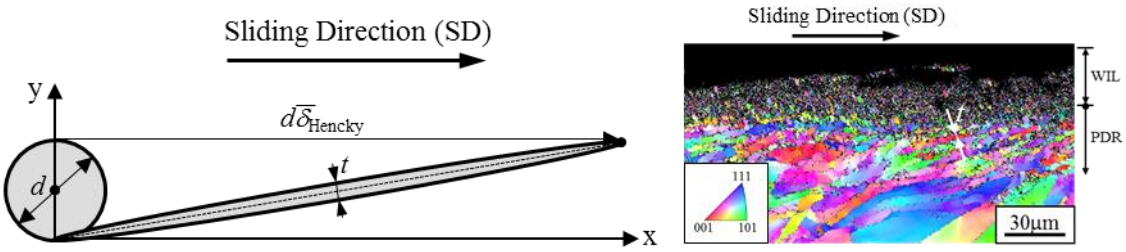

Fig. 10. (Color online) Schematic illustration showing simple shear deformation of an equiaxial grain together with micrograph of PDR of worn specimen with sliding distance of 1500 m.